Advances in Aircraft and Spacecraft Science, *Vol. 1, No. 3 (2014) 291-310*
DOI: http://dx.doi.org/10.12989/aas.2014.1.3.291

Flutter analysis by refined 1D dynamic stiffness elements and doublet lattice method

Alfonso Pagani*[1], Marco Petrolo[2a] and Erasmo Carrera[3b]

[1]*Department of Mechanical and Aerospace Engineering, Politecnico di Torino, Corso Duca degli Abruzzi 24, 10129 Torino, Italy*
[2]*School of Aerospace, Mechanical and Manufacturing Engineering RMIT University, Bundoora VIC 3083, Australia*
[3]*Department of Mechanical and Aerospace Engineering, Politecnico di Torino, Corso Duca degli Abruzzi 24, 10129 Torino, Italy*
Currently at SAMME, RMIT University, Melbourne, Australia

(Received March 7, 2013, Revised June 3, 2013, Accepted June 7, 2013)

Abstract. An advanced model for the linear flutter analysis is introduced in this paper. Higher-order beam structural models are developed by using the Carrera Unified Formulation, which allows for the straightforward implementation of arbitrarily rich displacement fields without the need of a-priori kinematic assumptions. The strong form of the principle of virtual displacements is used to obtain the equations of motion and the natural boundary conditions for beams in free vibration. An exact dynamic stiffness matrix is then developed by relating the amplitudes of harmonically varying loads to those of the responses. The resulting dynamic stiffness matrix is used with particular reference to the Wittrick-Williams algorithm to carry out free vibration analyses. According to the doublet lattice method, the natural mode shapes are subsequently used as generalized motions for the generation of the unsteady aerodynamic generalized forces. Finally, the g-method is used to conduct flutter analyses of both isotropic and laminated composite lifting surfaces. The obtained results perfectly match those from 1D and 2D finite elements and those from experimental analyses. It can be stated that refined beam models are compulsory to deal with the flutter analysis of wing models whereas classical and lower-order models (up to the second-order) are not able to detect those flutter conditions that are characterized by bending-torsion couplings.

Keywords: flutter; higher-order models; unified formulation; beams; doublet lattice method; dynamic stiffness method

1. Introduction

Aeroelasticity plays a critical role in the design of modern aerospace vehicles. Among others, flutter is one of the most important aeroelastic phenomena. Flutter can occur to a structure in a flow field, and it consists of undamped vibrations that can lead to catastrophic collapses. Different analysis tools have been developed to predict flutter after the publication of the now famous report

*Corresponding author, Ph.D. Student, E-mail: alfonso.pagani@polito.it
[a] Research Fellow, E-mail: marco.petrolo@rmit.edu.au
[b] Professor, E-mail: erasmo.carrera@polito.it

http://www.techno-press.org/?journal=aas&subpage=7 ISSN: 2287-528X (Print), 2287-5271 (Online)

by Theodorsen (1934), nearly 80 years ago. A vast range of aerodynamic models have been used in aeroelastic problems, from strip theories to Reynolds-averaged Navier-Stokes (RANS). Excellent reviews about these methodologies are presented in (Yurkovich 2003) and (Schuster *et al.* 2003). The doublet lattice method (DLM) emerged in the late 1960s (Albano and Rodden 1969). More recently, an improved version of DLM has been proposed by Rodden *et al.* (1998), and this version is used in this work. Three main features are responsible of DLM's success (Yurkovich 2003)

1. It offers good accuracy (unless transonic regimes are considered and/or separation occurs).
2. DLM is cost competitive with respect to simpler methods such as strip theories.
3. Fairly complex geometries can be analysed.

In this work, DLM has been coupled with a refined one-dimensional (1D) structural formulation for the flutter analysis of both isotropic and composite lifting surfaces. Beam models are widely used to analyse the mechanical behaviour of slender bodies, such as columns, rotor-blades and aircraft wings. The simplicity of 1D theories and their ease of application coupled with the computational efficiency are some of the main reasons that lead structural analysts to prefer them to two-dimensional (2D) and three-dimensional (3D) models. The classical and best-known beam theories that survived the test of time and are still valid to this day, are those by Euler (1744) - hereinafter referred to as EBBT - and Timoshenko (1922) – hereinafter referred to as TBT. The former does not account for transverse shear deformations and rotatory inertia, whereas the latter assumes a uniform shear distribution along the cross-section of the beam together with the effects of rotatory inertia. These models yield reasonably good results when slender, solid section, homogeneous structures are subjected to flexure. Conversely, the analysis of deep, thin-walled, open section beams may require more sophisticated theories to achieve sufficiently accurate results. An accurate aeroelastic analysis requires the proper detection of non-classical effects.

Many methods have been proposed to overcome the limitations of classical theories and to extend the application of 1D models to any geometry or boundary conditions (Novozhilov 1961). Early investigators have focused on the use of appropriate shear correction factors to increase the accuracy of classical 1D formulations, see for examples (Timoshenko and Goodier 1970). However, a review paper by Kaneko (1975) and a recent paper by Dong *et al.* (2010) highlighted the difficulty in the definition of a universally accepted formulation for shear correction factors. Another important class of refinement methods reported in the literature is based on the use of warping functions. The contributions by El Fatmi (2007) and Ladevéze *et al.* (2004) are some noteworthy examples. The variational asymptotic solution (VABS) was originated from the work by Berdichevsky *et al.* (1992). Some further valuable contributions about VABS are those by Volovoi *et al.* (1999) and Yu and Hodges (2004). Another important class of refined beam models are those based on the generalized beam theory (GBT) (Schardt 1994). GBT improves classical theories by using a piece-wise beam description of thin-walled sections and it has been widely discussed in the works by Silvestre (2007). Higher-order theories are generally obtained by using refined displacement fields of the beam cross-sections. Washizu (1968) ascertained how the use of an arbitrarily chosen rich displacement fields can lead to closed form exact 3D solutions. Many other higher-order theories have also been introduced to include non-classical effects. A review was compiled by Kapania and Raciti (1989a, b) focusing on flexural deformation, vibration analysis, wave propagations, buckling and post-buckling behaviour.

The aim of this work is to present aeroelastic models based on highly accurate 1D structural models and low-fidelity aerodynamic tools. An important effort to apply refined beam models to aeroelastic problems was made by Librescu and his co-workers who incorporated a number of

non-classical effects in order to study the static and dynamic aeroelastic response of beam structures (Librescu and Song 1992). In this paper, refined beam models are developed within the framework of the Carrera Unified Formulation (CUF) which is well established in the literature for over a decade (Carrera 1995, 2002, 2003). CUF is a hierarchical formulation that considers the order of the model, *N*, as a free-parameter (i.e. as an input) of the analysis or in other words, refined models are obtained without having the need for any ad hoc formulations. In the present work, beam theories using CUF (Carrera *et al.* 2011) are obtained on the basis of Taylor-type expansions (TE). EBBT and TBT can be obtained as particular or special cases. The strength of CUF TE 1D models in dealing with arbitrary geometries, thin-walled structures and identifying local effects are well known for both static (Carrera *et al.* 2012) and free-vibration analysis (Petrolo *et al*. 2012). In recent works, Varello *et al.* (2011) extended CUF 1D to steady aeroelasticity by using the Vortex Lattice Method (VLM), whereas DLM was used in (Petrolo 2012, 2013) in the framework of CUF for flutter analyses.

In majority of the papers on 1D CUF, the finite element method (FEM) has been used to handle arbitrary geometries and loading conditions. In the present work, a more powerful approach for CUF TE theories through the application of the Dynamic Stiffness Method (DSM) is provided and therefore used for the free vibration analysis of both metallic and laminated lifting surfaces. The mode shapes are then used with reference to DLM to carry out flutter analyses.

DSM has been recently extended to CUF theories in (Pagani *et al*. 2013, 2014), where a more comprehensive review on the use of DSM in structural dynamics can be found. The DSM is appealing in dynamic analysis because unlike the FEM, it provides the exact solution of the equations of motion of a structure once the initial assumptions on the displacements field have been made. This essentially means that, unlike the FEM and other approximate methods, the model accuracy is not unduly compromised when a small number of elements are used in the analysis. For instance, one single structural element can be used in the DSM to compute any number of natural frequencies to any desired accuracy. Of course, the accuracy of the DSM will be as good as the accuracy of the governing differential equations of the structural element in free vibration. In fact, the exact Dynamic Stiffness (DS) matrix stems from the solution of the governing differential equations. DSM has been quite extensively used for flutter analyses by Banerjee (2003), Butler and Banerjee (1996), Guo *et al.* (2003) and Lillico *et al.* (1997).

This paper is organized as follows: (i) first CUF is introduced and higher-order models are formulated, (ii) secondly, the principle of virtual displacements is used to derive the differential governing equations and the associated natural boundary conditions for the generic *N*-order model; (iii) next, the DSM is briefly discussed and the algorithm of Wittrick and Williams (1970) is used to compute the natural frequencies; (iv) subsequently, the mode shapes of metallic and composite lifting surfaces are computed and used as generalized motions for the generation of the DLM unsteady aerodynamic generalized forces; and (v) finally, the *g*-method (Chen 2000) is exploited to conduct flutter analyses.

2. Governing equations of the *N*-order beam model via CUF

The adopted rectangular Cartesian coordinate system is shown in Fig. 1. The cross-section of the beam lies on the xz-plane and it is denoted by Ω, whereas the boundaries over y are $0 \le y \le L$. Let us introduce the transposed displacement vector

$$\boldsymbol{u}(x,y,z;t) = \{u_x\, u_y\, u_z\}^T \tag{1}$$

Within the framework of the CUF, the 3D displacement field of Eq. (1) is expressed as

$$\boldsymbol{u}(x,y,z;t) = F_\tau(x,z)\,\boldsymbol{u}_\tau(y;t), \qquad \tau = 1,2,\ldots,M \tag{2}$$

where F_τ are the functions of the coordinates x and z on the cross-section. $\boldsymbol{u}_\tau$ is the vector of the generalized displacements, M stands for the number of the terms used in the expansion, and the repeated subscript, τ indicates summation. TE (Taylor Expansion) 1D CUF models consist of McLaurin series that uses the 2D polynomials $x^i z^j$ as F_τ functions, where i and j are positive integers. For instance, the displacement field of the second-order (N = 2) TE model can be expressed as

$$\begin{aligned} u_x &= u_{x_1} + x\,u_{x_2} + z\,u_{x_3} + x^2 u_{x_4} + xz\,u_{x_5} + z^2 u_{x_6} \\ u_y &= u_{y_1} + x\,u_{y_2} + z\,u_{y_3} + x^2 u_{y_4} + xz\,u_{y_5} + z^2 u_{y_6} \\ u_z &= u_{z_1} + x\,u_{z_2} + z\,u_{z_3} + x^2 u_{z_4} + xz\,u_{z_5} + z^2 u_{z_6} \end{aligned} \tag{3}$$

The order N of the expansion is set as an input of the analysis; the integer N is arbitrary and it defines the order of the beam theory. Classical Euler-Bernoulli (EBBT) and Timoshenko (TBT) beam theories can be realized as degenerated cases of the linear (N = 1) TE model. For further information about TE models see (Carrera *et al.* 2011).

In this paper, the principle of virtual displacement is used to derive the equations of motion.

$$\delta L_{int} = \int_V \delta \boldsymbol{\epsilon}^T \boldsymbol{\sigma}\, dV = -\delta L_{ine} \tag{4}$$

where $\boldsymbol{\epsilon}$ and $\boldsymbol{\sigma}$ are the strain and stress vectors, respectively. δL_{int} stands for the strain energy and δL_{ine} is the work done by the inertial loadings. δ stands as usual virtual variation operator. The virtual variation of the strain energy is rewritten using Eq. (2), the constitutive laws, and the linear strain-displacement relations. After integrations by part, Eq. (4) becomes

$$\delta L_{int} = \int_L \delta \boldsymbol{u}_\tau^T \boldsymbol{K}^{\tau s} \boldsymbol{u}_s\, dy + \left[\delta \boldsymbol{u}_\tau^T \boldsymbol{\Pi}^{\tau s} \boldsymbol{u}_s\right]_{y=0}^{y=L} \tag{5}$$

where $\boldsymbol{K}^{\tau s}$ is the differential linear stiffness matrix and $\boldsymbol{\Pi}^{\tau s}$ is the matrix of the natural boundary conditions in the form of 3 x 3 fundamental nuclei. The components of the nuclei are not given in the present work for the sake of brevity. They can be found in (Pagani *et al.* 2013, 2014).

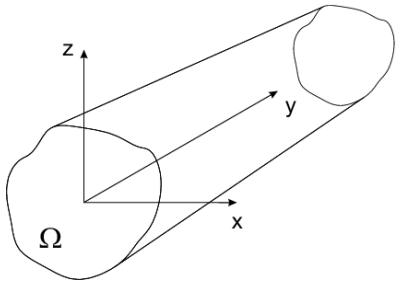

Fig. 1 Coordinate frame of the beam model

The virtual variation of the inertial loads is also rewritten in terms of the fundamental nucleus.

$$\delta L_{ine} = \int_L \delta \boldsymbol{u}_\tau \int_\Omega \rho F_\tau F_s \, d\Omega \, \ddot{\boldsymbol{u}}_s \, dy = \int_L \delta \boldsymbol{u}_\tau \boldsymbol{M}^{\tau s} \ddot{\boldsymbol{u}}_s \, dy \tag{6}$$

where ρ is the material density and $\boldsymbol{M}^{\tau s}$ is the fundamental nucleus of the mass matrix. Double over dots stand as second derivative with respect to time (t).

In the case of harmonic motion, the solution is sought in the form

$$\boldsymbol{u}_s(y;t) = \boldsymbol{U}_s(y) e^{i\omega t} \tag{7}$$

where $\boldsymbol{U}_s(y)$ is the amplitude function of the motion, ω is an arbitrary circular frequency, and i is $\sqrt{-1}$. Eq. (7) allows the formulation of the equilibrium equations and the natural boundary conditions in the frequency domain. In a matrix form, the equations of motion can be expressed as follow

$$\delta \boldsymbol{U}_\tau : \boldsymbol{L}^{\tau s} \widetilde{\boldsymbol{U}}_s = 0 \tag{8}$$

where

$$\widetilde{\boldsymbol{U}}_s = \left\{ U_{xs} \quad U_{xs,y} \quad U_{xs,yy} \; U_{ys} \quad U_{ys,y} \; U_{ys,yy} \; U_{zs} \quad U_{zs,y} \; U_{zs,yy} \right\}^T \tag{9}$$

The suffix after the comma denotes the derivatives. $\boldsymbol{L}^{\tau s}$ is the 3×9 matrix that contains the coefficients of the ordinary differential equations. The component of $\boldsymbol{L}^{\tau s}$ are provided below and they are referred to as $L^{\tau s}_{(i\,j)}$, where i is the row number and j is the column number

$$\begin{aligned}
&L^{\tau s}_{(11)} = -\omega^2 E^{\rho}_{\tau s} + E^{(22)}_{\tau_{,x^s},x} + E^{(44)}_{\tau_{,z^s},z} && L^{\tau s}_{(12)} = E^{(26)}_{\tau_{,x^s}} - E^{(26)}_{\tau s,_x} && L^{\tau s}_{(13)} = -E^{66}_{\tau s} \\
&L^{\tau s}_{(14)} = E^{(26)}_{\tau_{,x^s},x} + E^{(45)}_{\tau_{,z^s},z} && L^{\tau s}_{(15)} = E^{(23)}_{\tau s,_x} - E^{(66)}_{\tau s,_x} && L^{\tau s}_{(16)} = -E^{36}_{\tau s} \\
&L^{\tau s}_{(17)} = E^{(12)}_{\tau_{,x^s},z} + E^{(44)}_{\tau_{,z^s},x} && L^{\tau s}_{(18)} = E^{(45)}_{\tau_{,z^s}} - E^{(16)}_{\tau s,_z} && L^{\tau s}_{(19)} = 0 \\
&L^{\tau s}_{(21)} = E^{(26)}_{\tau_{,x^s},x} + E^{(45)}_{\tau_{,z^s},z} && L^{\tau s}_{(22)} = E^{(66)}_{\tau_{,x^s}} - E^{(23)}_{\tau s,_x} && L^{\tau s}_{(23)} = -E^{36}_{\tau s} \\
&L^{\tau s}_{(24)} = -\omega^2 E^{\rho}_{\tau s} + E^{(66)}_{\tau_{,x^s},x} + E^{(55)}_{\tau_{,z^s},z} && L^{\tau s}_{(25)} = E^{(36)}_{\tau_{,x^s}} - E^{(36)}_{\tau s,_x} && L^{\tau s}_{(26)} = -E^{33}_{\tau s} \\
&L^{\tau s}_{(27)} = E^{16}_{\tau_{,x^s},z} + E^{45}_{\tau_{,z^s},x} && L^{\tau s}_{(28)} = E^{(55)}_{\tau_{,z^s}} - E^{(13)}_{\tau s,_z} && L^{\tau s}_{(29)} = 0 \\
&L^{\tau s}_{(31)} = E^{44}_{\tau_{,x^s},z} + E^{12}_{\tau_{,z^s},x} && L^{\tau s}_{(32)} = E^{(16)}_{\tau_{,z^s},x} - E^{(45)}_{\tau s,_z} && L^{\tau s}_{(33)} = 0 \\
&L^{\tau s}_{(34)} = E^{45}_{\tau_{,x^s},z} + E^{16}_{\tau_{,z^s},x} && L^{\tau s}_{(35)} = E^{(13)}_{\tau_{,z^s}} - E^{(55)}_{\tau s,_z} && L^{\tau s}_{(36)} = 0 \\
&L^{\tau s}_{(37)} = -\omega^2 E^{\rho}_{\tau s} + E^{44}_{\tau_{,x^s},x} + E^{11}_{\tau_{,z^s},z} && L^{\tau s}_{(38)} = E^{(45)}_{\tau_{,x^s}} - E^{(45)}_{\tau s,_x} && L^{\tau s}_{(26)} = -E^{55}_{\tau s}
\end{aligned} \tag{10}$$

The generic term $E^{\alpha\beta}_{\tau,\theta s,\xi}$ above is a cross-sectional moment parameter

$$E^{\alpha\beta}_{\tau,\theta s,\xi} = \int \widetilde{C}_{\alpha\beta} F_{\tau,\theta} F_{s,\xi} \, d\Omega \tag{11}$$

with $\widetilde{C}_{\alpha\beta}$ a material coefficient. Conversely, the parameter $E^{\rho}_{\tau s}$ is

$$E^{\rho}_{\tau s} = \int_{\Omega} \rho F_{\tau} F_{s} d\Omega \tag{12}$$

For a given expansion order, N, the equilibrium equations of the generic beam theory can be obtained in the form of Eq. (13) as given below by expanding $\boldsymbol{L}^{\tau s}$ for τ and s ranging from 1 to $M = (N+1)(N+2)/2$ as shown in Fig. 2. It reads

$$\boldsymbol{L}\widetilde{\boldsymbol{U}} = 0 \tag{13}$$

In a similar way, the boundary conditions can be written in a matrix form as

$$\delta \boldsymbol{U}_{\tau} : \boldsymbol{P}_{s} = \boldsymbol{B}^{\tau s}\, \hat{\boldsymbol{U}}_{s} \tag{14}$$

where $\boldsymbol{P}_{\mathrm{s}}$ is the generalised loading vector and

$$\hat{\boldsymbol{U}}_{\mathbf{s}} = \left\{ U_{xs} \quad U_{xs,_y} \quad U_{ys} \quad U_{ys,_y} \quad U_{zs} \quad U_{zs,_y} \right\}^{T} \tag{15}$$

$\boldsymbol{B}^{\tau s}$ is the 3 x 6 matrix that contains the coefficient of the natural boundary conditions

$$\boldsymbol{B}^{\tau s} = \begin{bmatrix} E^{26}_{\tau s,_x} & E^{66}_{\tau s} & E^{66}_{\tau s,_x} & E^{36}_{\tau s} & E^{16}_{\tau s,_z} & 0 \\ E^{23}_{\tau s,_x} & E^{36}_{\tau s} & E^{36}_{\tau s,_x} & E^{33}_{\tau s} & E^{13}_{\tau s,_z} & 0 \\ E^{45}_{\tau s,_z} & 0 & E^{55}_{\tau s,_z} & 0 & E^{45}_{\tau s,_z} & E^{55}_{\tau s} \end{bmatrix} \tag{16}$$

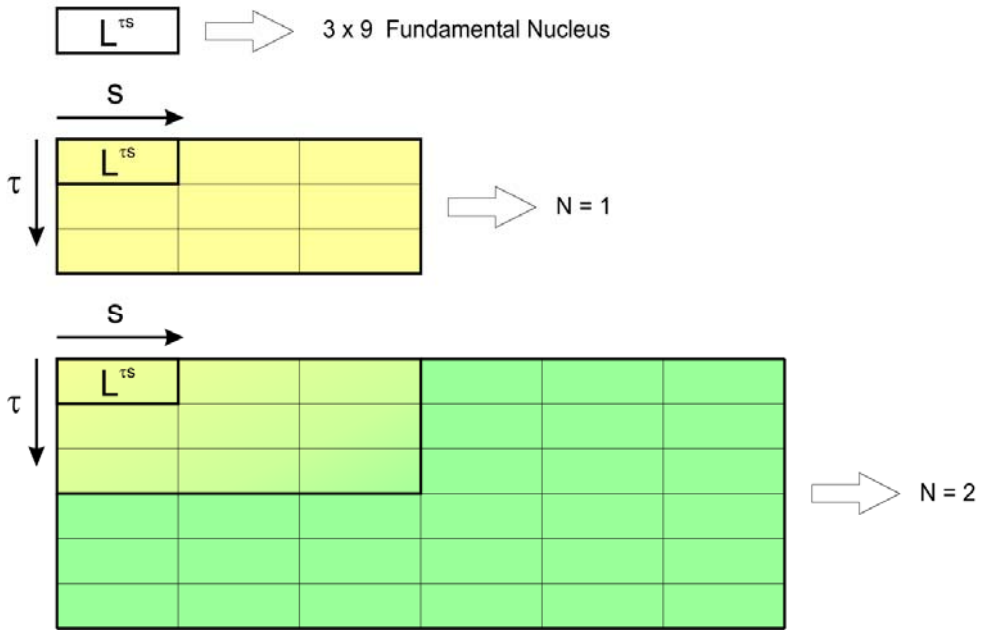

Fig. 2 Expansion of the matrix $\boldsymbol{L}^{\tau s}$ for a given expansion order

For a given expansion order, matrix $\boldsymbol{B}^{ts}$ is expanded in the same way as $\boldsymbol{L}^{ts}$ to finally give

$$\boldsymbol{P} = \boldsymbol{B}\hat{\boldsymbol{U}} \tag{17}$$

3. The dynamic stiffness method

Eq. (13) is a system of ordinary differential equations (ODEs) of second-order in y with constant coefficients. A change of variables is used to reduce the second order system of ODEs to a first-order system,

$$\boldsymbol{Z} = \{Z_1 \;\; Z_2 \;\; \ldots \;\; Z_n\}^T = \hat{\boldsymbol{U}} \tag{18}$$

where $\hat{\boldsymbol{U}}$ is the expansion of $\hat{\boldsymbol{U}}_s$ (see Eq. (15)) for a given expansion order and n = 6 x M is the dimension of the unknown vector as well as the number of differential equations. In (Pagani *et al.* 2013), an automatic algorithm to transform the $\boldsymbol{L}$ matrix of Eq. (13) into the matrix $\boldsymbol{S}$ of the following linear differential system was described

$$\boldsymbol{Z}_{,\mathrm{y}}(\mathrm{y}) = \boldsymbol{S}\boldsymbol{Z}(\mathrm{y}) \tag{19}$$

Once the differential problem is described in terms of Eq. (19), the solution can be written as follows

$$\boldsymbol{Z} = \boldsymbol{\delta}\boldsymbol{C}\,\mathrm{e}^{\boldsymbol{\lambda}\mathrm{y}} \tag{20}$$

where $\boldsymbol{\lambda}$ is the vector of the eigenvalues of $\boldsymbol{S}$. The element δ_{ij} of matrix $\boldsymbol{\delta}$ is the j-th component of the i-th eigenvector of matrix $\boldsymbol{S}$ and the vector $\boldsymbol{C}$ contains the integration constants that need to be determined by using the boundary conditions.

Once the closed form analytical solution has been found, the generic boundary conditions for the generalized displacements and forces need to be applied (see Fig. 3). It should be noted that the vector $\boldsymbol{Z}$ of Eq. (20) does not only contain the displacements but also their first derivatives. If only displacements are needed, by recalling Eq. (20), only the lines $1,3,5,\ldots,n-1$ should be taken into account. Therefore, by evaluating Eq. (20) in 0 and L and applying the boundary conditions as

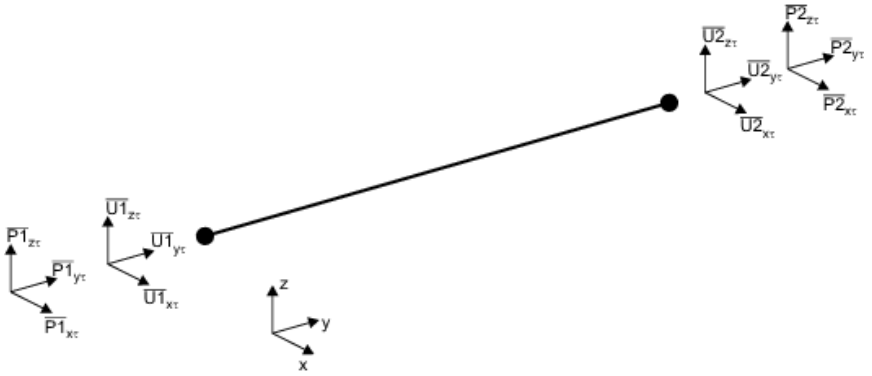

Fig. 3 Boundary conditions of the beam element and sign conventions

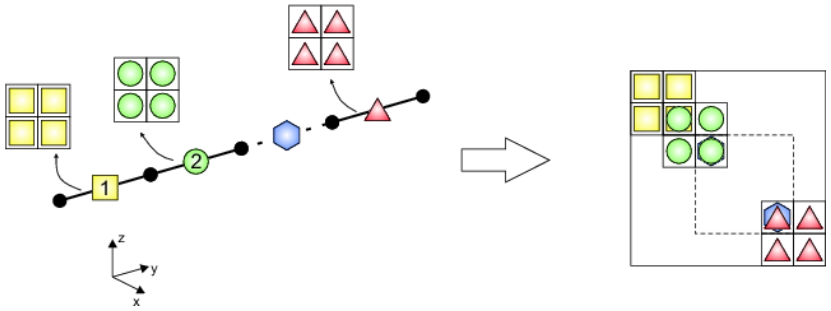

Fig. 4 Assembly of dynamic stiffness matrices

shown in Fig. 3, the following matrix relation for the nodal displacements is obtained

$$\overline{\boldsymbol{U}} = \boldsymbol{A}\,\boldsymbol{C} \tag{21}$$

Similarly, boundary conditions for generalized nodal forces are written as follows

$$\overline{\boldsymbol{P}} = \boldsymbol{R}\,\boldsymbol{C} \tag{22}$$

$\overline{\boldsymbol{U}}$ and $\overline{\boldsymbol{P}}$ are the vectors of the amplitudes of the harmonically varying nodal generalized displacements and loads, respectively. Matrices $\boldsymbol{A}$ and $\boldsymbol{R}$ are not given here for the sake of brevity, but they can be found in (Pagani *et al.* 2013, 2014).

The constant vector $\boldsymbol{C}$ from Eqs. (21) and (22) can now be eliminated to give the DS matrix of the element as follows

$$\overline{\boldsymbol{P}} = \boldsymbol{K}\overline{\boldsymbol{U}} \tag{23}$$

where

$$\boldsymbol{K} = \boldsymbol{R}\,\boldsymbol{A}^{-1} \tag{24}$$

is the required frequency dependant DS matrix.

The DS matrix given above is the basic building block to compute the exact natural frequencies of a higher-order beam. The DSM has also many of the general features of the FEM. In particular, it is possible to assemble elemental DS matrices to form the overall DS matrix of any complex structures consisting of beam elements (see Fig. 4).

Once the global DS matrix of the final structure is obtained, the boundary conditions can be applied by using the well-known penalty method (often used in FEM) or by simply removing rows and columns of the stiffness matrix corresponding to the degrees of freedom which are zeroes.

3.1 Natural frequencies and mode shapes computation

For free vibration analysis of structures, FEM generally leads to a linear eigenvalue problem. By contrast, the DSM leads to a transcendental (non-linear) eigenvalue problem for which the Wittrick-Williams algorithm (Wittrick and Williams 1970) is recognisably the best available solution technique at present. The basic working principle of the algorithm can be briefly summarised in the following steps:

- A trial frequency ω^* is chosen to compute the DS matrix $\boldsymbol{K}^*$
- $\boldsymbol{K}^*$ is reduced to its upper triangular form by the usual form of Gauss elimination to obtain $\boldsymbol{K}^{*\Delta}$ and the number of negative terms on the leading diagonal of $\boldsymbol{K}^{*\Delta}$ is counted; this is known as the sign count $s(\boldsymbol{K}^*)$ of the algorithm;
- The number, j, of natural frequencies (ω) of the structure which lie below the trial frequency (ω^*) is given by

$$j = j_0 + s(\boldsymbol{K}^*) \tag{25}$$

j_0 is the number of natural frequencies of all individual elements with clamped-clamped (CC) boundary conditions on their opposite sides which still lie below the trial frequency ω^*. Note that j_0 is required because the DSM allows for an infinite number of natural frequencies to be accounted for when all the nodes of the structure are fully clamped so that one or more individual elements of the structure can still vibrate on their own between the nodes. Assuming that j_0 is known, and $s(\boldsymbol{K}^*)$ can be obtained by counting the number of negative terms in $\boldsymbol{K}^{*\Delta}$, a suitable procedure can be devised, for example the bi-section method, to bracket any natural frequency between an upper and lower bound of the trial frequency ω^* to any desired accuracy.

Once the natural frequency has been computed and the related global DS matrix evaluated, the corresponding nodal generalized displacements can be obtained by solving Eq. (23) for a random vector of nodal generalized forces. The integration constants $\boldsymbol{C}$ can then be computed with the help of Eq. (21). In this way, using Eq. (20), the unknown generalized displacements can be computed as a function of y. Finally, by using Eqs. (7) and (2), the complete displacement field can be generated as a function of x, y, z and the time t.

4. Doublet lattice method and mesh-to-mesh transformations

Following Landahl (1967) or Albano and Rodden (1969), the normalwash in a point with coordinates x, y due to the pulsating pressure jump Δp in the point ξ, η has the following expression

$$\overline{w} = \frac{1}{8\pi}\int_A \overline{\Delta p}\, K(x_0, y_0, \omega, M)\, dA \tag{26}$$

where M is the Mach number, ω is the circular frequency and

$$x_0 = x - \xi; \quad y_0 = y - \eta \tag{27}$$

The kernel function (K) formal expression is not reported here for the sake of brevity, it can be found in (Landahl 1967). Eq. (26) can be numerically solved by means of the Doublet Lattice Method (DLM). In the DLM framework a lifting surface is discretized in a number of panels and the following algebraic system of equations has to be solved

$$\overline{w}_i = \sum_{j=1}^{N_{AP}} D_{ij}\, \overline{\Delta p}_j \tag{28}$$

where N_{AP} indicates the total number of aerodynamic panels and D_{ij} is the normal wash factor. In this paper D_{ij} was calculated by exploiting Rodden's quartic DLM (Rodden *et al.* 1998). For

the sake of brevity, the procedure to compute the normalwash factor is not reported here, it can be found in Rodden's paper. It is important to underline that the steady contribution to D_{ij} was computed via the Vortex Lattice Method (VLM) (Katz and Plotkin 1991).

The unsteady aeroelastic analysis was carried out by considering a set of modal shapes as generalized motions for the unsteady aerodynamic generalized force generation. Each set of modal shapes, $\boldsymbol{\phi}_m$ was defined on a set of points above the structure. Slopes and displacements at control and load points of the aerodynamic panels are then given by

$$\frac{\partial \mathrm{Z_m}}{\partial x} = \boldsymbol{A}\,\boldsymbol{\phi}_m \tag{29}$$

$$\widetilde{\mathrm{Z}}_\mathrm{m} = \widetilde{\boldsymbol{A}}^*\,\boldsymbol{\phi}_m \tag{30}$$

$$\mathrm{Z_m} = \boldsymbol{A}^*\,\boldsymbol{\phi}_m \tag{31}$$

where $\widetilde{Z}_m$ and Z_m are the displacements at load and control points, respectively. $\boldsymbol{A}$, $\widetilde{\boldsymbol{A}}^*$ and $\boldsymbol{A}^*$ were computed through the Infinite Plate Spline (IPS) (Harder and Desmarais 1972). For the sake of brevity, the explicit expressions of these matrices are not reported here, they can be found in (Demasi and Livne 2009). IPS was chosen in order to better exploit the shell-like capabilities of the present 1D structural formulation, as shown by Varello *et al.* (2011). Under the assumption of simple harmonic motion, it is possible to demonstrate that the vector that contains the normalized (using the velocity V_∞ parallel to x) normal wash has the following expression (the boundary condition is enforced on all control points of the lifting surface)

$$\mathbf{w}_\mathrm{m} = i\frac{\omega}{V_\infty}\mathrm{Z_m} + \frac{\partial \mathrm{Z_m}}{\partial x} \tag{32}$$

where all the vector quantities have to be understood as vectors of amplitudes of the harmonic motion and i is the imaginary unit.

5. Generalized matrices and *G*-method

The generalized aerodynamic matrix for a given reduced frequency (k) is given by

$$Q_{ij}(ik) = \sum_{N=1}^{N_{AP}} \Delta p_j^N(ik)\,\widetilde{Z}_i^N\,A^N \tag{33}$$

- $k = \omega b/L$, b is the reference length (equal to the half of the reference chord) and L is the length of the structure.
- $\Delta p_j^N(ik)$ is the pressure jump due to the *j*-th set of motions (modal shapes), acting on the N -th aerodynamic panel and evaluated for a given reduced frequency. The computation of the pressure jump is performed by means of the DLM.
- $\widetilde{Z}_i^N$ is the i -th motion set evaluated at the *N*-th aerodynamic panel. Starting from the i -th modal shape given by a structural model, the *i*-th motion set is then mapped on the aerodynamic panels by means of the splining process. In this work, modal shapes were evaluated by means of CUF 1D models and DSM.

- A^N is the area of the N-th panel.

$\boldsymbol{Q}(ik)$ is a square matrix with N_{modes} x N_{modes} elements, where N_{modes} indicates the total number of natural modes adopted. Typically, N_{modes} ranges from 10 to 20.

The generalized mass matrix is given by

$$\tilde{\boldsymbol{M}} = \boldsymbol{\phi}\, \boldsymbol{M}\, \boldsymbol{\phi} \tag{34}$$

where

- $\boldsymbol{\phi}$ is a matrix containing a given number of modal shapes, dimension: N_{DOF} x N_{modes}. N_{DOF} is the total number of DOFs of the structural model.
- $\boldsymbol{M}$ is the mass matrix of the structure (dimension: N_{DOF} x N_{DOF}), $\boldsymbol{M}$ is a square diagonal matrix with N_{modes} x N_{modes} terms.

In the case of DSM as in this paper, matrix $\boldsymbol{M}$ is evaluated as follows

$$\boldsymbol{M} = \frac{\boldsymbol{K} - \boldsymbol{K}(\omega_i)}{\omega_i^2} \tag{35}$$

where $\boldsymbol{K}$ is the ("static") structural matrix and it is evaluated as the DS matrix of Eq. (24), $\boldsymbol{K}$, at null frequency. ω_i is the oscillatory frequency associated to the i-th modal shape.

The generalized stiffness matrix is a square diagonal (N_{modes} x N_{modes}) matrix. Its diagonal terms are given by

$$\tilde{K}_{ii} = \omega_i^2\, \tilde{M}_{ii} \tag{36}$$

The g-method was introduced by Chen (2000) and it is based on a damping perturbation technique and a first-order model of the damping term. Its derivation exploits the aerodynamics in the Laplace domain and can be found in (Chen 2000). The basic assumption of the *g*-method is based on the following approximation of the generalized aerodynamic matrix

$$\tilde{\boldsymbol{Q}}(p) \approx \tilde{\mathbf{Q}}(ik) + g\tilde{\mathbf{Q}}'(ik), \quad \text{for} \quad g << 1 \tag{37}$$

Where $g = \gamma^k$ and γ is the transient decay rate coefficient. Eq. (37) leads to the g-method equation

$$\left[\left(\frac{V_\infty}{b}\right)^2 \tilde{\boldsymbol{M}}\, p^2 + \tilde{\boldsymbol{K}} - \frac{1}{2}\rho V_\infty^2\, \tilde{\boldsymbol{Q}}'(ik) g - \frac{1}{2}\rho V_\infty^2\, \tilde{\boldsymbol{Q}}(ik)\right]\{\boldsymbol{q}(p)\} = 0 \tag{38}$$

where p is the nondimensional Laplace parameter ($p = g + ik$) and b is is the reference length (usually equal to the half of the reference chord).

The generalized aerodynamic matrix, $\tilde{\boldsymbol{Q}}(ik)$, is provided by the unsteady aerodynamic model (DLM) in the frequency domain. The computation of $\tilde{\boldsymbol{Q}}'(ik)$ has to be performed numerically. A central difference scheme can be used and a forward one at $k = 0$. Three new matrices are introduced

$$\boldsymbol{A} = \left(\frac{V_\infty}{b}\right)^2 \tilde{\boldsymbol{M}} \tag{39}$$

$$\boldsymbol{B} = 2ik\left(\frac{V_\infty}{b}\right)^2 \widetilde{\boldsymbol{M}} - \frac{1}{2}\rho V_\infty^2 \widetilde{\boldsymbol{Q}}'(ik)$$

$$\mathbf{C} = -k^2\left(\frac{V_\infty}{b}\right)^2 \widetilde{\boldsymbol{M}} + \widetilde{\boldsymbol{K}} - \frac{1}{2}\rho V_\infty^2 \widetilde{\boldsymbol{Q}}'(ik)$$

Eq. (38) therefore becomes

$$\left[g^2\,\boldsymbol{A} + g\,\boldsymbol{B} + \boldsymbol{C}\right]\{\boldsymbol{q}\} = 0 \tag{40}$$

This is a second-order linear system in g; the g-method targets to find those solutions having $Im(g) = 0$. Eq. (40) is rewritten in the state-space form,

$$\left[\boldsymbol{D} - g\,\boldsymbol{I}\right]\{\boldsymbol{X}\} = 0 \tag{41}$$

where

$$\boldsymbol{D} = \begin{bmatrix} \mathbf{0} & \boldsymbol{I} \\ -\boldsymbol{A}^{-1}\boldsymbol{C} & -\boldsymbol{A}^{-1}\boldsymbol{B} \end{bmatrix} \tag{42}$$

6. Results and discussion

Numerical assessments were carried out on isotropic and composite structures. Fig. 5 shows the sweep and fiber orientation angles (positive directions). An 8 × 30 aerodynamic mesh was exploited since this mesh offers good accuracy as shown by Petrolo (2012, 2013). The first ten natural modes were used to build the generalized matrices.

6.1 Isotropic plate wing

An isotropic wing modeled as a flat plate was first considered. The wing model that was investigated has the following characteristics: $L = 0.305$ m, $c = 0.076$ m, and thickness $t = 0.001$ m.

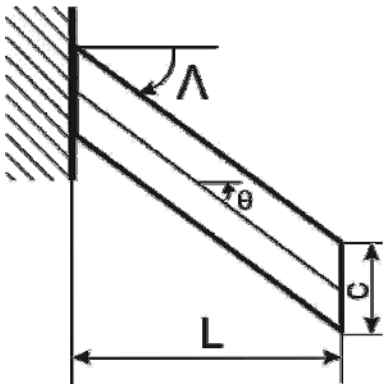

Fig. 5 Sweep and fiber orientation angles

The material is an aluminum alloy with elastic modulus $E = 73.8$ GPa, shear modulus $G = 27.6$ GPa and density $\rho = 2768$ Kg/m^3. This model was retrieved from (Koo 2001).

Table 1 shows the first three natural frequencies for a swept back configuration ($\Lambda = 30°$). Different beam models were considered, classical (EBBT and TBT) and higher-order (from $N = 1$ to $N = 4$). The results that were obtained through the present DSM approach were compared with FEM results that were obtained by Petrolo (2012). Bending and torsional modes were detected.

Table 2 shows the flutter velocity of the forward swept configuration ($\Lambda = -30°$). Again, the DSM was compared against FEM (Petrolo 2012) and the influence of the beam model was evaluated. The results from the classical and the linear ($N = 1$) models were not reported since no flutter conditions were detected by those models. In fact, as it is clear from Table 1, the classical and the linear ($N = 1$) structural models are not able to foresee torsion and coupling phenomena, which are fundamental in flutter analysis.

Table 1 Effect of the CUF 1D expansion order (N) on the vibration frequencies (Hz) of the isotropic plate wing by means of DSM and FEM, $\Lambda = 30°$

Model	Method	f_1	f_2	f_3
EBBT	FEM	8.967	56.192	157.335
	DSM	8.968	56.191	157.336
TBT	FEM	8.966	56.189	157.320
	DSM	8.967	56.190	157.320
$N = 1$	FEM	8.966	56.185	157.308
	DSM	8.965	56.186	157.308
$N = 2$	FEM	7.199	44.462	97.939*
	DSM	7.180	44.338	97.863*
$N = 3$	FEM	7.125	43.778	74.316*
	DSM	7.105	43.654	74.412*
$N = 4$	FEM	7.093	43.529	73.296*
	DSM	7.070	43.389	73.370*

*Torsional mode

Table 2 Effect of the CUF 1D expansion order (N) on the flutter velocities of the isotropic plate wing by means of DSM and FEM, $\Lambda = -30°$

Model	Method	Velocity (m/s)
$N = 2$	FEM	84.206
	DSM	84.086
N = 3	FEM	59.202
	DSM	59.366
$N = 4$	FEM	58.050
	DSM	58.188

Table 3 Flutter velocities of the isotropic plate wing for different sweep angles by means of DSM and FEM, $N = 4$ model

Λ	Method	Velocity (m/s)
-30°	FEM	58.050
	DSM	58.186
-20°	FEM	51.109
	DSM	51.560
-10°	FEM	46.029
	DSM	46.371
0°	FEM	68.406
	DSM	68.523
10°	FEM	64.262
	DSM	64.506
20°	FEM	60.684
	DSM	59.130
30°	FEM	57.339
	DSM	57.216

The influence of the sweep angle on the flutter velocity is reported in Table 3. On the other hand, the influence of the beam models on the flutter condition is shown in Tables 4-5. Finally, Fig. 6 shows the damping and the frequency of the first three modes versus the free-stream velocity of the swept back wing. From Fig. 6, it is clear that flutter occurs as the damping crosses the zero-line and the first two modes coalesce. The following comments stem from the results that were obtained for the isotropic case:

- The 1D DSM results perfectly match the FEM solutions. Since in (Petrolo 2012) the FEM solutions by means of CUF 1D models were successfully compared against those ones by 2D plate models (Koo 2001), it can be stated that the present 1D DSM models can detect flutter conditions of wings with plate-like accuracy.
- At least a third-order beam model ($N = 3$) is needed to have reliable flutter analyses. This is due to the need of a proper description of torsion and of the bending-torsion coupling to detect flutter conditions.
- The $N = 3$ and $N = 4$ models provide similar results. This means that the convergence to the exact solution with respect to the beam order is almost obtained.
- The $N = 2$ model provides reliable results for moderate or null sweep angles.
- The classical models and $N = 1$ cannot predict flutter conditions in which torsion and coupling effects are predominant.

6.2 Composite plate wing

In the second analysis case, composite wing structures were considered. Composite plate wing models were retrieved from (Kameyama and Fukunaga 2007) and from (Hollowell and Dugundji 1984). A graphite/epoxy composite material with the following characteristics was used: $E_L = 98.0$ *GP*a, $E_T = 7.90$ *GP*a, $G_{LT} = 5.60$ *GP*a, Poisson ratio $\nu = 0.28$ and $\rho = 1520$ Kg/m^3,

where L denotes the fibers direction and T a direction perpendicular to the fibers. The length of the wing (L) is equal to 305 mm and the chord (c) is equal to 76.2 mm. The total thickness of the laminate is 0.804 mm.

Table 4 Effect of the expansion order (N) on the flutter velocity (m/s) of the isotropic plate wing by means of DSM

Λ	$N = 2$	$N = 3$	$N = 4$
-30°	84.086	59.366	58.188
-20°	64.769	51.559	51.559
-10°	49.676	46.210	46.371
0°	69.388	68.503	68.523
10°	65.441	64.305	64.506
20°	66.408	61.046	59.130
30°	70.145	57.747	57.216

Table 5 Effect of the expansion order (N) on the flutter frequency (Hz) of the isotropic plate wing by means of DSM

Λ	$N = 2$	$N = 3$	$N = 4$
-30°	64.773	52.181	51.668
-20°	61.616	56.737	56.581
-10°	62.020	59.816	59.746
0°	40.002	39.029	38.995
10°	38.362	37.361	37.352
20°	36.736	35.095	34.793
30°	34.156	31.887	31.616

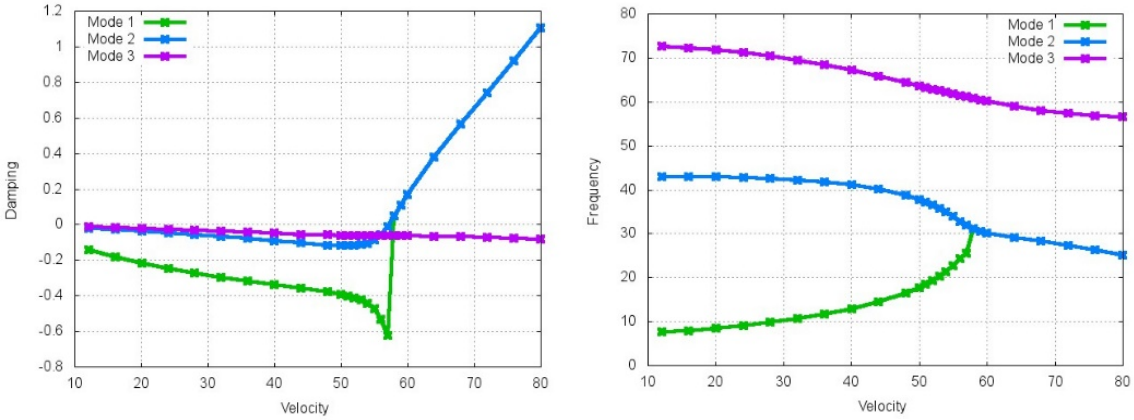

(a) Damping vs velocity (b) Frequency vs velocity

Fig. 6 Mode frequency and damping vs free-stream velocity for the isotropic plate wing, $\Lambda = 30°$, fourth-order ($N = 4$) DSM model

Table 6 Flutter velocities (m/s) for a six-layer straight plate wing. DSM CUF beam vs CLT (Kameyama and Fukunaga 2007) and experimental (Hollowell and Dugundji 1984) results

Stacking	$N = 2$	$N = 3$	$N = 4$
$[0_2/90]_s$ CLT, 23.0 EXP, 25	23.3	23.3	23.2
$[45/-45/0]_s$ CLT, 40.1 EXP, > 32	43.3	40.4	40.4
$[45_2/0]_s$ CLT, 27.5 EXP, 28	32.5	26.9	26.7
$[30_2/0]_s$ CLT, 27.1 EXP, 27	29.3	26.3	26.3

Table 7 Natural frequencies (Hz) and flutter velocities (m/s) of an eight-layer straight plate wing via different models

Model	f_1	f_2	f_3	f_4	f_5	V_F
$N = 2$	7.4	46.1*	59.1	129.5*	182.7	38.2
$N = 3$	7.2	45.1*	59.1	126.5*	182.4	38.2
$N = 4$	7.2	45.0*	59.1	126.4*	182.3	38.1
CLT (Kameyama and Fukunaga 2007)	7.3	45.4*	59.1	127.7*	182.3	38.8

*Torsional mode

Table 8 Natural frequencies (Hz) and flutter velocities (m/s) of an eight-layer swept ($\Lambda = 30°$) plate wing via different models

Model	f_1	f_2	f_3	f_4	f_5	V_F
N = 2	5.6	34.7	76.5*	97.5	193.3*	38.6
N = 3	5.6	34.4	60.1*	95.9	187.0*	31.5
N = 4	5.6	34.2	59.2*	95.3	180.1*	31.7
CLT (Kameyama and Fukunaga 2007)	5.6	34.4	60.0*	95.4	182.0*	32.4

*Torsional mode

First, symmetric six-layer laminates with constant thickness layers were considered. The plate wing was straight ($\Lambda = 0°$). Table 6 shows the flutter velocities for various stacking sequences and various beam models. The results from the present DSM refined elements were compared with those from CLT (Classical Laminate Theory) plate models and with experimental results from the literature.

An eight-layer symmetric stacking sequence was then considered. The stacking sequence was equal to $[-22.5/67.5/22.5/-67.5]_s$, whereas the thickness sequence was $[0.09/0.12/0.16/0.63]_s$, where each term indicates the thickness ratio of each ply with respect to the half of the thickness of the laminate. For instance, the thickness of the first layer is the 9% of the half thickness of the laminate. Two sweep angles were considered, $\Lambda = 0°$ and $\Lambda = 30°$. The natural frequencies and the

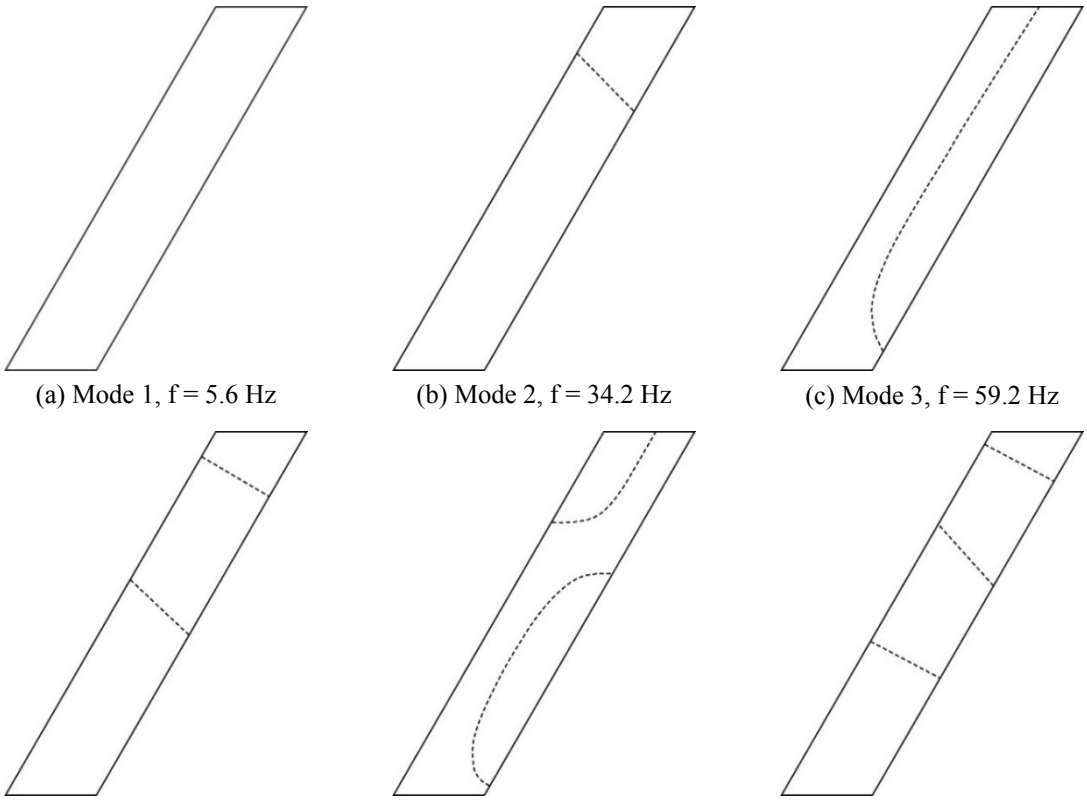

(a) Mode 1, f = 5.6 Hz (b) Mode 2, f = 34.2 Hz (c) Mode 3, f = 59.2 Hz

(d) Mode 4, 95.3 Hz (e) Mode 5, f = 180.1 Hz (f) Mode 6, 185.7 Hz

Fig. 7 Modal shapes of the 8-layer swept plate wing, $N = 4$ DSM model

flutter velocities are given in Tables 7 and 8, in which the results from the present variable order 1D DSM models are compared with those from plates and from experiments. Finally, the nodal lines of the first sixth mode shapes of the swept wing ($\Lambda = 30°$) via the $N = 4$ DSM beam model are shown in Fig. 7. The composite case analysis suggests that

- The present 1D DSM results perfectly match the 2D CLT results. A good agreement with the experimental results was also found.
- It is confirmed that at least an $N = 3$ beam model should be used to predict flutter.
- The $N = 2$ model can be used for un-swept configurations.
- The classical and the $N = 1$ models are not able to detect flutter.
- It is definitely demonstrated that the proposed method allow for accurate and efficient flutter analysis of both isotropic and composite plate wings.

7. Conclusions

This paper has presented aeroelastic analyses that were carried out by means of advanced beam models. The aeroelastic equations of motions have been solved by coupling the structural models – exact 1D refined Dynamic Stiffness beam elements – with the DLM. Furthermore, the *g*-method

was exploited to detect the flutter conditions. Isotropic and composite plate wings have been considered. The influence of the sweep angle was also investigated. The results have been compared against 1D CUF FEM models, 2D plate models and experimental results available from the literature. The fundamental role played by the beam order in flutter detection has been pointed out. The results that have been obtained draw the following conclusions

- The present 1D DSM approach provides results that perfectly match those ones from 1D and 2D FEM. A good agreement with the experimental results was also found.
- The adoption of refined beam models is compulsory to detect flutter. This is due to the influence of the bending-torsion coupling. Such a coupling cannot be modelled through the classical beam models that cannot therefore predict flutter.
- The uncompromising accuracy of the Dynamic Stiffness Method coupled with the 1D Carrera Unified Formulation represent a very powerful and reliable tool for aeroelastic analyses. Its strength is due to its hierarchical capabilities that allow the user to set the beam order as an input of the analyses. The exact solution can be easily found through a convergence analysis.
- Future investigations should be carried out on the aeroelastic analysis of more complex wing configurations and the coupling of the 1D CUF models with higher-fidelity CFD tools could be considered.

References

Albano, E. and Rodden, W.P. (1969), "A doublet-lattice method for calculating lift distributions on oscillating surfaces in subsonic flows", *AIAA J.*, **7**(2), 279-285.

Banerjee, J.R. (2003), "A simplified method for the free vibration and flutter analysis of bridge decks", *J. Sound Vib.*, **260**(5), 829-845.

Butler, R. and Banerjee, J.R. (1996), "Optimum design of bending-torsion coupled beams with frequency or aeroelastic constraints", *Comput. Struct.*, **60**(5), 715-724.

Berdichevsky, V.L., Armanios, E. and Badir, A. (1992), "Theory of anisotropic thin-walled closed-cross section beams", *Compos. Part B. Eng.*, **2**(5-7), 411-432.

Carrera, E. (1995), "A class of two dimensional theories for multilayered plates analysis", *Atti Accademia delle Scienze di Torino, Memorie Scienze Fisiche*, **19-20**, 49-87.

Carrera, E. (2002), "Theories and finite elements for multilayered, anisotropic, composite plates and shells", *Arch. Comput. Method. E.*, **9**(2), 87-140.

Carrera, E. (2003), "Theories and finite elements for multilayered plates and shells: A unified compact formulation with numerical assessment and benchmarking", *Arch. Comput. Method. E*, **10**(3), 216-296.

Carrera, E., Giunta, G. and Petrolo, M. (2011), *Beam Structures: Classical and Advanced Theories*, John Wiley & Sons.

Carrera, E., Petrolo, M. and Zappino, E. (2012), "Performance of CUF approach to analyze the structural behavior of slender bodies", *J. Struct. Eng-ASCE*, **138**(2), 285-297.

Chen, P.C. (2000), "Damping perturbation method for flutter solution: The *g*-method", *AIAA J.*, **38**(9), 1519-1524.

Demasi, L. and Livne, E. (2009), "Dynamic aeroelasticity of structurally nonlinear configurations using linear modally reduced aerodynamic generalized forces", *AIAA J.*, **47**(1), 71-90.

Dong, S.B., Alpdongan, C. and Taciroglu, E. (2010), "Much ado about shear correction factors in Timoshenko beam theory", *Int. J. Solids Struct.*, **47**(13), 1651-1665.

El Fatmi, R. (2007), "Non-uniform warping including the effects of torsion and shear forces. Part I: A General beam theory", *Int. J. Solids Struct.*, **44**(18-19), 5912-5929.

Euler, L. (1744), *De Curvis Elasticis*, Lausanne and Geneva, Bousquet..

Guo, S.J., Banerjee, J.R. and Cheung, C.W. (2003), "The effect of laminate lay-up on the flutter speed of composite wings", *Proceedings of the Institution of Mechanical Engineers, Part G: J. Aerospace Eng,*, **217**(3), 115-122.

Harder, R.L. and Desmarais, R.N. (1972), "Interpolation using surface splines", *J. Aircraft*, **9**(2), 189-192.

Hollowell S.J. and Dugundji, J. (1984), "Aeroelastic flutter and divergence of stiffness coupled, graphite/epoxy cantilevered plates", *J. Aircraft*, **21**(1), 69-76.

Kameyama, M. and Fukunaga, H. (2007), "Optimum design of composite plate wings for aeroelastic characteristics using lamination parameters", *Comput. Struct.*, **85**(3-4), 213-224.

Kaneko, T. (1975), "On Timoshenko's correction for shear in vibrating beams", *J. Phys. D. Appl. Phys.*, **8**(16), 1927-1936.

Kapania, K. and Raciti, S. (1989a), "Recent advances in analysis of laminated beams and plates, Part I: shear effects and buckling", *AIAA J.*, **27**(7), 923-935.

Kapania, K. and Raciti, S. (1989b), "Recent advances in analysis of laminated beams and plates, Part II: vibrations and wave propagation", *AIAA J.*, **27**(7), 935-946.

Katz, J. and Plotkin, A. (1991), *Low-Speed Aerodynamics: From Wing Theory to Panel Methods*, McGraw-Hill, Inc., New York.

Koo, K.N. (2001), "Aeroelastic characteristics of double-swept isotropic and composite wings", *J. Aircraft*, **38**(2), 343-348.

Ladéveze, P., Sanchez, P. and Simmonds, J. (2004), "Beamlike (Saint-Venant) solutions for fully anisotropic elastic tubes of arbitrary closed cross-section", *Int. J. Solids Struct.*, **41**(7), 1925-1944.

Landahl, M.T. (1967), "Kernel function for nonplanar oscillating surfaces in a subsonic flow", *AIAA J.*, **5**(5), 1045-1046.

Librescu, L and Song, O. (1992), "On the static aeroelastic tailoring of composite aircraft swept wings modelled as thin-walled beam structures", *Compos. Eng.*, **2**(5-7), 497-512.

Lillico, M., Butler, R., Guo, S. and Banerjee, J.R. (1997), "Aeroelastic optimisation of composite wings using the dynamic stiffness method". *Aeronaut. J.*, **101**(1002), 77-86.

Novozhilov, V.V. (1961), *Theory of Elasticity*, Pergamon Press, Oxford, 1961.

Pagani, A., Boscolo, M., Banerjee, J.R. and Carrera, E. (2013), "Exact dynamic stiffness elements based on one dimensional higher-order theories for free vibration analysis of solid and thin-walled structures", *J. Sound Vib.*, **332**(23), 6104-6127. DOI: 10.1016/j.jsv.2013.06.023.

Pagani, A., Carrera, E., Boscolo, M. and Banerjee, J.R. (2014), "Refined dynamic stiffness elements applied to free vibration analysis of generally laminated composite beams with arbitrary boundary conditions", *Compos. Struct.*, **110**, 305-316. DOI: 10.1016/j.compstruct.2013.12.010.

Petrolo, M. (2012), "Advanced 1D structural models for flutter analysis of lifting surfaces", *Int. J. Aeronautical Space Sci.*, **13**(2), 199-209.

Petrolo, M. (2013), "Flutter analysis of composite lifting surfaces by the 1D Carrera unified formulation and the doublet lattice method", *Compos. Struct.*, **95**(8), 539-546.

Petrolo, M., Zappino, E. and Carrera, E. (2012), "Refined free vibration analysis of one-dimensional structures with compact and bridge-like cross-sections", *Thin-Wall. Struct.*, **56**, 49-61.

Rodden, W.P., Taylor, P.F. and McIntosh, S.C.J. (1998), "Further refinement of the subsonic doublet-lattice method", *J. Aircraft*, **35**(5), 720-726.

Schardt, R. (1994), "Generalized beam theory an adequate method for coupled stability problems", *Thin-Wall. Struct.*, **19(2-4)**, 161-180.

Schuster, D.M., Liu, D.D. and Huttsell L.J. (2003), "Computational aeroelasticity: Success, progress, challenge", *J. Aircraft*, **40**(5), 843-856.

Silvestre, N. (2007), "Generalised beam theory to analyse the buckling behaviour of circular cylindrical shells and tubes", *Thin-Wall. Struct.*, **45**(2), 185-198.

Theodorsen, T. (1934), "General theory of aerodynamic instability and the mechanism of flutter", *NACA Rept. 496*.

Timoshenko, S.P. (1922), "On the corrections for shear of the differential equation for transverse vibrations

of prismatic bars", *Philos. Mag.*, **41**, 744-746.
Timoshenko, S.P. and Goodier, J.N. (1970), *Theory of Elasticity*, McGraw-Hill.
Varello, A., Carrera, E. and Demasi, L. (2011), "Vortex lattice method coupled with advanced one-dimensional structural models", *J. Aeroelasticity Struct. Dyn.*, **2**(2), 53-78.
Volovoi, V.V., Hodges, D.H., Berdichevsky, V.L. and Sutyrin, V.G. (1999), "Asymptotic theory for static behaviour of elastic anisotropic I-beams", *Int. J. Solids Struct.*, **36**(7), 1017-1043.
Washizu, K. (1968), "Variational Methods in Elasticity and Plasticity", Pergamon, Oxford.
Wittrick, W.H. and Williams, F.W. (1970), "A general algorithm for computing natural frequencies of elastic structures", *Q. J. Mech. Appl. Math.*, **24**(3), 263-284.
Yu, W. and Hodges, D.H. (2004), "Elasticity solutions versus asymptotic sectional analysis of homogeneous, isotropic, prismatic beams", *J. Appl. Mech.*, **71**(1), 15-23.
Yurkovich, R. (2003), "Status of unsteady aerodynamic prediction for flutter of high-performance aircraft", *J. Aircraft*, **40**(5), 832-842.

EC